Available online at www.sciencedirect.com
ScienceDirect
Trans. Nonferrous Met. Soc. China 30(2020) 2413−2423
Transactions of Nonferrous Metals Society of China
www.tnmsc.cn

Comparison on corrosion resistance and surface film of pure Mg and Mg−14Li alloy

Chuan-qiang LI, Zhi-pei TONG, Yi-bin HE, Huai-pei HUANG, Yong DONG, Peng ZHANG

School of Materials and Energy, Guangdong University of Technology, Guangzhou 510006, China

Received 25 December 2019; accepted 20 June 2020

Abstract: To study different corrosion resistances and surface film types of hexagonal close-packed (HCP) pure Mg and body-centered cubic (BCC) Mg−14wt.%Li alloy in 0.1 mol/L NaCl, a series of experiments were conducted, including hydrogen evolution, mass loss, in-situ electrochemical testing combined with Raman spectroscopy and microstructural observation. The results indicate that the corrosion resistance of pure Mg is superior to that of Mg−14Li, and the protective function of the surface films on both magnesium systems is elevated within 16 h of immersion in 0.1 mol/L NaCl. An articulated, thick, and needle-like surface film containing Li_2CO_3 on Mg−14Li, different from the typically thin, flaky $Mg(OH)_2$ film on pure Mg, is confirmed via scanning electron microscopy (SEM). However, both surface films can be broken down at a high anodic over-potential. Thus, different corrosion resistances of the two Mg systems are ascribed to various protective films forming on their surfaces.

Key words: Mg−Li alloy; corrosion resistance; surface film; electrochemical testing; in-situ electrochemical-Raman spectroscopy

1 Introduction

Magnesium (Mg) is an electrochemically and chemically active metal. Thus, it readily reacts with the atmosphere in humid environments [1−4]. Generally, a thicker outer layer of $Mg(OH)_2$ and a thinner inner layer of MgO are deposited on the surface of hexagonal close-packed (HCP) Mg alloys in NaCl solution [5−7]. The compactness and protective function of the surface film on magnesium are characterized by the Pilling−Bedworth ratio (PBR) [8,9]. A PBR less than one indicates that the film formed to protect the magnesium is insufficient [9]. Furthermore, the PBR also reflects the stress state of surface film, i.e., a tensile stress developed in the film with PBR <1, and compressive stress developed in the film with PBR >1 [8,9]. Therefore, a significant deviation of the PBR to one can cause cracking and spallation of the surface film due to large growth stress in the surface film [8]. The PBR of $Mg(OH)_2$ film (1.8) is greater than 1, whereas the PBR of MgO film (0.8) is lower than 1 [9]. The PBR bias of $Mg(OH)_2$ film is higher, while MgO film is uncompacted and also reacted with water to form hydroxide [6,10,11]. Consequently, the surface film of $Mg(OH)_2$ cannot protect the magnesium effectively.

Although alloying elements can modify the composition of the surface film on magnesium to some extent [12−14], the protective function of the surface film on traditional HCP Mg is still insignificant during the long-term corrosion process [12]. Furthermore, the addition of alloying elements to magnesium generally causes inclusions and/or second phases, resulting in a high

Foundation item: Projects (51901047, 51801029) supported by the National Natural Science Foundation of China; Projects (201911845185, xj201911845345) supported by the National College Students Innovation and Entrepreneurship Training Program, China

Corresponding author: Chuan-qiang LI; Tel: +86-13060861457; E-mail: cqli13s@alum.imr.ac.cn

DOI: 10.1016/S1003-6326(20)65388-2

degradation rate induced by galvanic corrosion between the matrix and inclusions/second phases [15−17]. The corrosion resistance of high purity Mg is superior to that of Mg alloying systems [17]. Regarding application, in practice, alloying Mg is also an effective approach to achieving a balance between mechanical and corrosion performance [18,19]. Although alloying lithium alters the crystal structure (HCP structure: <5.5 wt.% Li, HCP + body-centered cubic (BCC) duplex structure: 5.5−10.3 wt.% Li, BCC structure: >10.3 wt.% Li) and effectively improves the ductility of magnesium alloys, their corrosion resistance is closely correlated with their lithium content [4,20].

Recently, many works have shown that the BCC Mg−Li system presents ultra-high corrosion resistance in NaCl solution because its surface is covered by Li_2CO_3 and other compounds, which have attracted researchers' attention [20,21]. YAN et al [22−24] identified the specific properties of the protective film on the multi-alloy Mg−Li−Al−Y−Zr. The multi-layered film comprises an outermost Li_2CO_3 layer, a porous layer comprised of needle-shaped $Mg(OH)_2$, a thin intermediate layer containing a relatively intense signal of Al, and a more compact inner layer containing $Mg(OH)_2$, MgO, as well as Li_2CO_3 and Mg hydroxy-carbonate [22−24]. Furthermore, surface dissolution of a BCC Mg−Li−Al−Y−Zr alloy can be suppressed quickly after damage, which is consistent with the notion that a so-called self-healing, protective film can form on BCC Mg−Li alloys in an aqueous solution [22]. In addition, the enhanced protective function of the surface film on binary BCC Mg−14Li alloy with prolonged exposure time to NaCl solution has also been reported in previous work [21]. Therefore, the BCC Mg−Li system can be classified as a high-corrosion-resistant Mg alloy, which can guide the future design of high-strength alloying magnesium with a concomitant high corrosion- resistant BCC matrix.

Previous studies have primarily focused on Mg and Mg−Li alloys containing alloying element, resulting in an ambiguous understanding on the intrinsic nature of the surface film on HCP Mg and BCC Mg−Li due to the effect of alloying elements and/or secondary phases in the matrix. In particular, the composition and the deposition process of binary BCC Mg−Li alloys without additional elements are unclear to date. In this study, to further deepen the fundamental understanding of the corrosion and surface films in the entire Mg system, pure HCP Mg and BCC Mg−14Li are used to eliminate other possible influences (e.g., second phases). As a combination of electrochemical and Raman testing is an effective approach to identify specific properties of the surface film on metal materials [23,25], an in-situ Raman−electro-chemical technique is configurated to study the surface film formed on the pure HCP Mg and BCC Mg−14Li alloy during cathodic and anodic polarization.

2 Experimental

The raw material was highly pure Mg with a nominal purity of 99.95 wt.%. Binary Mg−14Li alloy with a nominal composition of approximately 86.25 wt.% magnesium and 13.66 wt.% lithium was fabricated via vacuum induction furnace using high purity Mg and Li ingots. The purity of pure magnesium and the compositions Mg−14Li alloy were analyzed by inductively coupled plasma atomic emission spectrum (ICP-AES). To eliminate casting defects, the Mg−14Li alloy was extruded into a plate with a cross-sectional size of 50 mm × 15 mm at about 350 °C. Sample pieces cut from the pure Mg ingot and Mg−14Li plate were ground with silicon carbide (SiC) papers to a 5000 grit finish and then finely polished to a 1 μm finish with ethanol. Phase analysis was conducted by a D/Max 2400 X-ray diffraction (XRD) system using monochromatic Cu K_α radiation, a step size of 0.02° and a scan rate of 1 (°)/min.

To study corrosion performance, samples with 12 mm × 10 mm × 3 mm dimensions were immersed in 0.1 mol/L neutral NaCl solution (pH=6.9) for a specific duration at room temperature. The corroded surface was observed using optical microscopy (OM) and scanning electron microscopy (SEM, JEOL−7100F). For hydrogen evolution experiments, samples with 15 mm × 15 mm × 6 mm dimensions were immersed in 0.1 mol/L NaCl solution (open to air) for 24 h at room temperature. Hydrogen gas was collected via an inverted funnel and burette above the immersed specimens. Mass loss tests were also performed for 3 days in 0.1 mol/L NaCl at room temperature for samples with surfaces

prepared to a 2000 grit using SiC paper. Afterwards, samples were cleaned to remove corrosion products from surface using a chromic acid solution of 200 g/L chromium trioxide, 10 g/L silver nitrate and 20 g/L barium nitrate.

Potentiodynamic polarization measurements were carried out with a scan rate of 1 mV/s by using a Bio-Logic VMP−3Z potentiostat. A conventional three-electrode electrochemical configuration was employed with platinum as counter electrode, saturated calomel electrode (SCE) as reference electrode and the samples with an exposed area of 1 cm^2 as working electrode. The measurements were performed in 0.1 mol/L NaCl solution at room temperature. To assess the electrochemical properties of surface film on the pure Mg and Mg−14Li, potentiodynamic polarization and electrochemical impedance spectroscopy (EIS) was conducted following 10 min, 8 h and 16 h immersion in 0.1 mol/L NaCl. The scan frequency of EIS was carried out over a frequency range from 100 kHz to 10 mHz with 10 mV of amplitude of sinusoidal potential signals with respect to the OCP. The EIS spectra were fitted using ZSimpWin 3.30 software. In all cases, at least three replicated tests for each electrochemical test were performed to ensure the reproducibility. To analyze the corrosion films on the pure Mg and Mg−14Li matrix, Raman spectroscopy was performed by using confocal microscopy system (WITec, alpha 300R) with 50 objective (NA=0.9) in an ambient condition. The 532 nm laser was used to excite samples that were placed on a piezo crystal-controlled scanning stage. The spectra were collected using 1800 line/mm grating. To clarify the deposited compounds on the surface in real time, the in-situ configuration combined with the electrochemical and Raman tests was set up.

3 Results and discussion

3.1 Microstructure and corrosion resistance

X-ray diffraction (XRD) results show that the pure Mg and Mg−14Li alloy are composed of HCP α-Mg and BCC β-Li, respectively, as shown in Fig. 1. For comparison of the corrosion behaviors of the pure Mg and Mg−14Li, the hydrogen evolution, mass loss rate and corroded surface of pure Mg and Mg−14Li subjected to 24 h immersion in 0.1 mol/L NaCl solution are shown in Fig. 2. Compared with conventional Mg alloys, both the pure Mg and the Mg−14Li alloy exhibit a low hydrogen evolution rate [26], indicating the superior corrosion resistance of a pure matrix (HCP or BCC structure). Generally, the cathodic second phases and/or impurity caused by the alloying process are considered to be the key in the corrosion performance of a Mg matrix [27,28]. In addition, persistent Li_2CO_3 compounds can be deposited to effectively protect the BCC Mg−Li matrix, mitigating the detrimental effect of lithium alloying [20]. In this work, it is notable that the hydrogen evolution rate of pure Mg with an HCP matrix is lower than that of BCC Mg−14Li with a BCC matrix, concomitant with localized dark corrosion products on the surface (Fig. 2(d)). To further assess the corrosion resistance of the pure Mg and Mg−14Li alloy, mass loss testing was also conducted and the results show that the corrosion rate of pure Mg is lower than that of binary Mg−14Li alloy (Fig. 2(b)). Therefore, the corrosion resistance of high purity Mg is better than that of Mg−14Li alloy in this study.

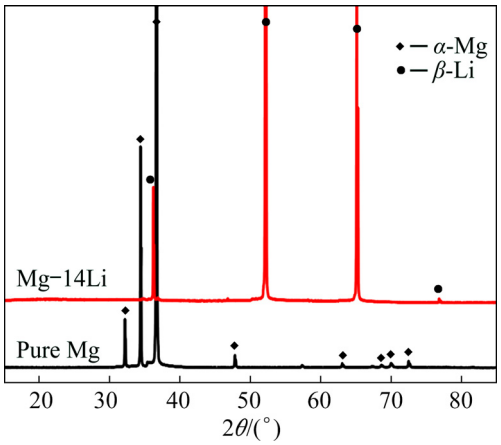

Fig. 1 X-ray diffraction (XRD) spectra of pure Mg and Mg−14Li alloy

3.2 Electrochemical testing

Electrochemical testing after immersion in 0.1 mol/L NaCl for different time intervals (OCP retention) shows the corrosion resistance of surface film deposited on the matrix and potentiodynamic polarization curves of the pure Mg and the Mg−14Li alloy are shown in Fig. 3. The polarization characteristics of the pure Mg are: (1) cathodic kinetics is essentially unaffected by the conditioning time in 0.1 mol/L NaCl, which is varied from 10 min to 8 h and then 16 h;

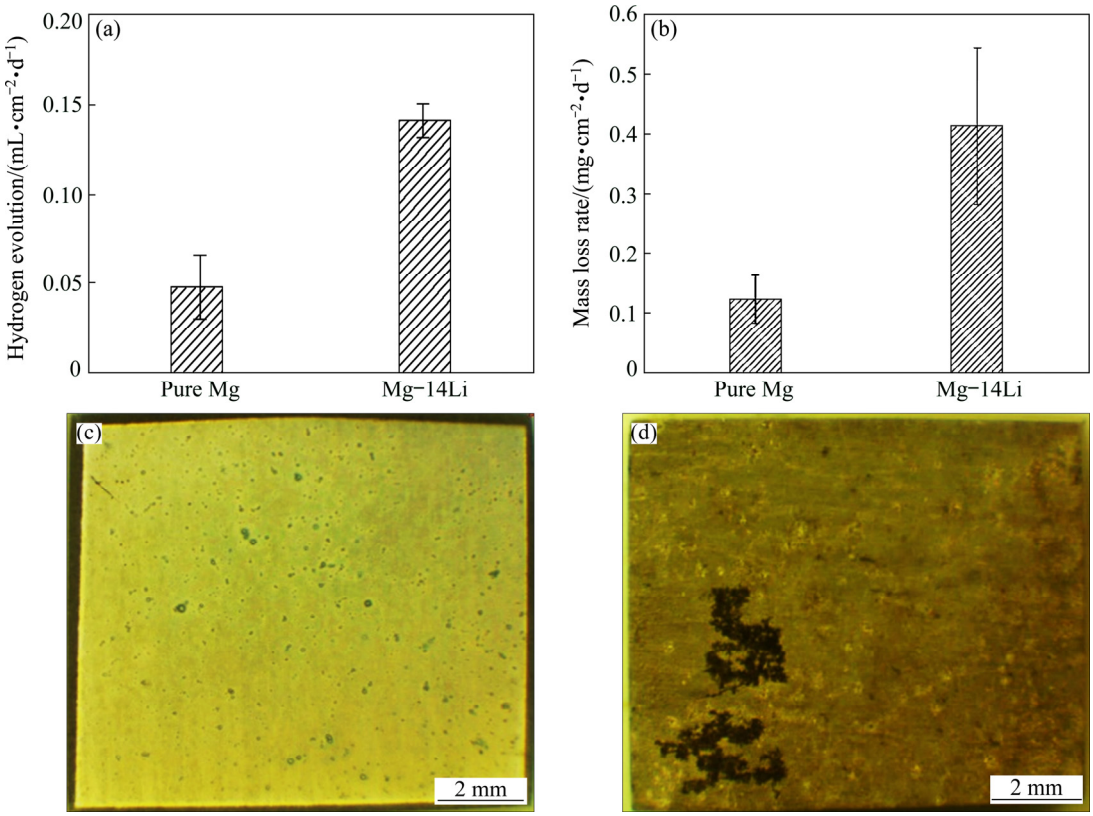

Fig. 2 Hydrogen evolution (a), mass loss rate (b) and corroded surface of pure Mg (c) and Mg−14Li (d) alloy after 24 h immersion in 0.1 mol/L NaCl

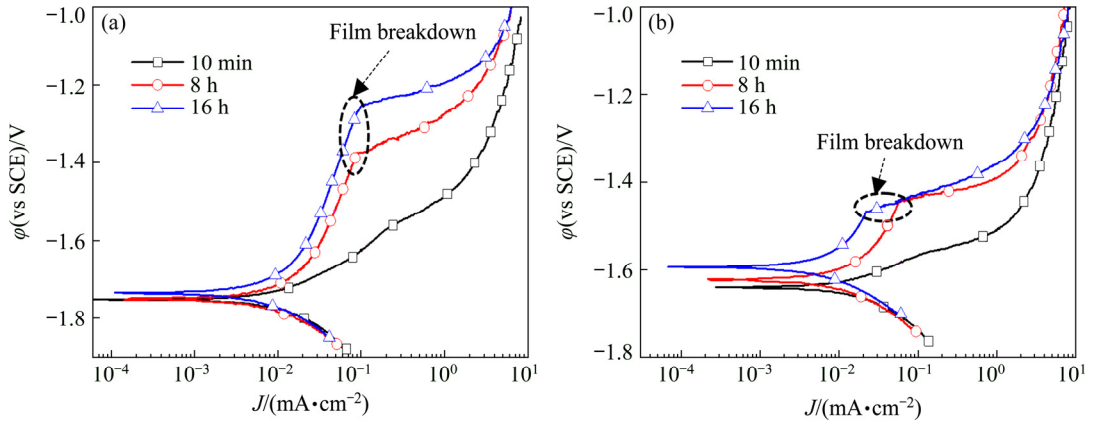

Fig. 3 Potentiodynamic polarization curves of pure Mg (a) and Mg−14Li alloy (b) exposed to 0.1 mol/L NaCl for different OCP conditioning periods

(2) dissolution (anodic) current for relatively low anodic overpotentials gradually decreases with increasing exposure time, concomitant with the temporal increase in the anodic Tafel slope from 10 min to 8 h to 16 h; (3) a distinct film breakdown potential (−1.4 V vs SCE) is noted in response to anodic polarization conditions for 8 h, and the breakdown potential (−1.25 V vs SCE) is further elevated after the OCP holding time is prolonged to 16 h. The polarization characteristics of pure Mg demonstrate that a time- dependent surface film formation occurs, which does not influence cathodic kinetics, nor provides a kinetic barrier to anodic dissolution. It appears that the elevated corrosion resistance of HCP Mg in this study contradicts the commonly held concept that Mg has poor corrosion resistance [29]. However, the high electrochemical corrosion property of pure Mg herein is attributed to the purified matrix (excluding heteroatoms) subjected to weakened ion exchange in dilute NaCl solution. In contrast, the surface film of $Mg(OH)_2$, which is insoluble naturally, retains its

protective capacity for an extended period. For the alloyed magnesium, the protective $Mg(OH)_2$ is present but only for a short time because of the enhanced electrochemical or chemical reaction induced by cathodic inclusion and/or second phases, which has been elucidated in previous works [30,31]. Similar polarization characteristics as those of pure Mg are detected in BCC Mg−14Li after immersion for different time, but the breakdown potential (−1.45 V vs SCE) for 16 h immersion remains almost constant when compared with that for 8 h immersion. Meanwhile, the current density reduces slightly with the increase of immersion time. In essence, the surface film on Mg−14Li alloy is sensitive to corrosion current, whereas the surface film on pure HCP Mg is sensitive to corrosion potential. However, it can be speculated that the surface film on the BCC Mg−14Li alloy is prone to stabilizing rapidly, but endures a low anodic over-potential in NaCl solution.

To further study the corrosion surface film of the two magnesium specimens, electrochemical impedance spectroscopy (EIS) tests were conducted in 0.1 mol/L NaCl solution and the results are shown in Fig. 4. The Nyquist plots of the pure Mg

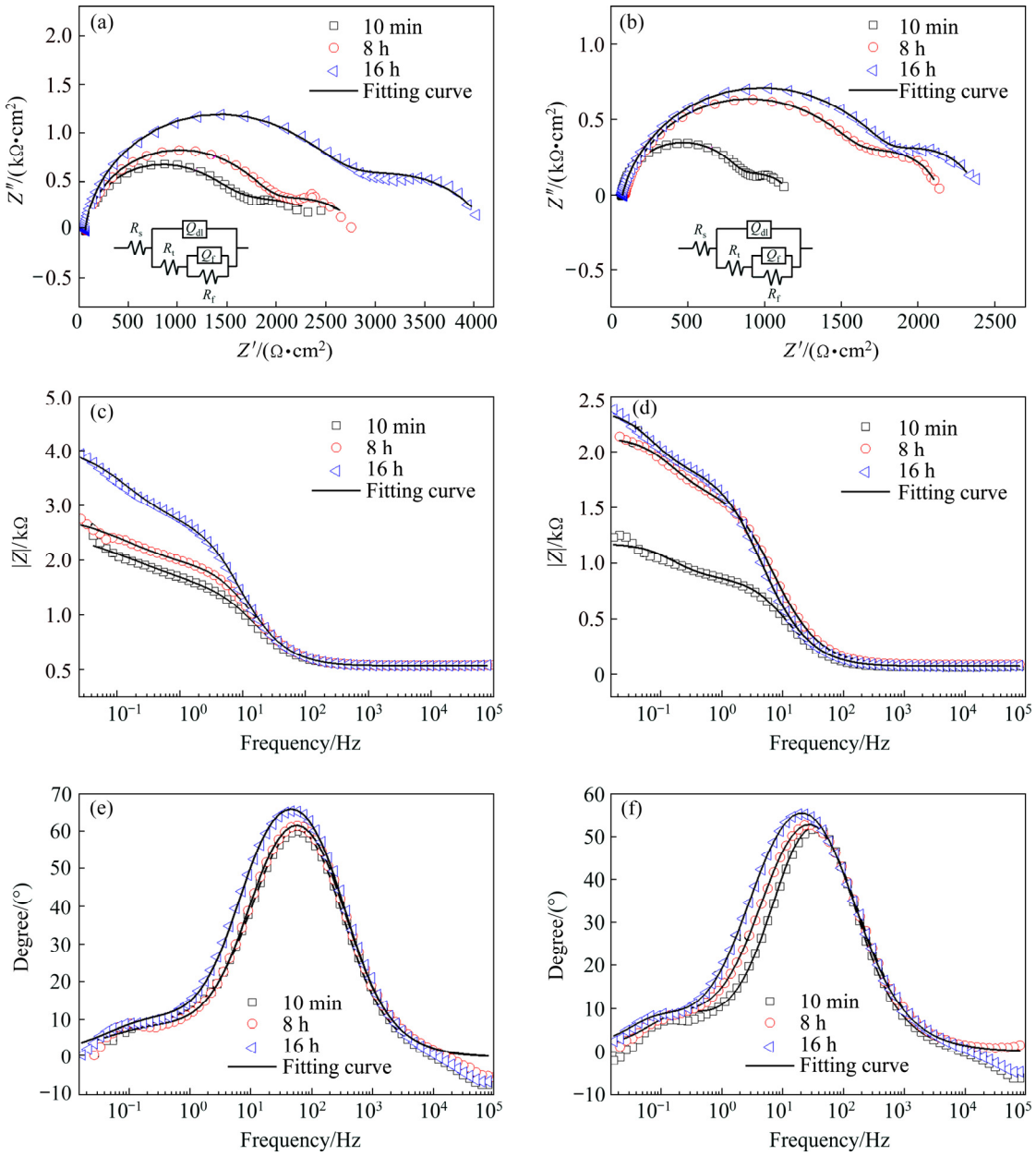

Fig. 4 EIS spectra of pure Mg (a, c, e) and Mg−14Li alloy (b, d, f) exposed to 0.1 mol/L NaCl solution for different OCP conditioning periods: (a, b) Nyquist plots; (c, d) Bode plots of $|Z|$ vs frequency; (e, f) Bode plots of degree vs frequency

and the Mg−14Li alloy subjected to different OCP conditioning periods consist of one large high−medium frequency capacitance loop and one small low frequency capacitance loop. The high frequency capacitance loops are ascribed to the electric double layer at the interface between the Mg substrate and the electrolyte, while the low frequency capacitance loops are related to the surface film [32]. In addition, the diameter of the capacitance loops for the pure Mg and the Mg−14Li alloy is enlarged with increasing OCP holding time. In general, the large capacitance loop indicates the low dissolution rate [31,32]. On the other hand, the low frequency inductance loops appear generally for conventional magnesium alloys due to corrosion nucleation at the initiation stage of localized corrosion [31,33]. However, the absence of an inductive loop is unique in the Nyquist response of Mg alloy during EIS testing in dilute chloride solution in this study. Therefore, the protective function of the surface film on the matrix of the pure Mg and the Mg−14Li alloy is elevated after short-term immersion in 0.1 mol/L NaCl solution. Furthermore, the size of the loops for pure Mg is larger than that for Mg−14Li alloy, indicating a better corrosion performance of pure Mg, which is inconsistent with the results from hydrogen evolution and mass loss rate (Fig. 2).

In terms of the Bode plots of $|Z|$ versus frequency (Figs. 4(b) and (e)), the impedance values consistently rise from a high frequency to low frequency for pure Mg and Mg−14Li alloy within the testing time. Moreover, the impedance values of pure Mg are larger than those of Mg−14Li alloy. For the Bode plots of degree versus frequency (Figs. 4(c) and (f)), besides a small wave crest observed in the low frequency range, a large wave crest is visible for pure Mg and Mg−14Li alloy under all conditions in the high frequency range, indicating the presence of two capacitance loops. Thus, the EIS results demonstrate that the corrosion resistance of the two specimens composed of pure HCP and BCC matrix increases with the immersion time during 16 h of immersion due to the formation of a surface film, which is in agreement with the results from the polarization curves.

For further comparison of the corrosion characteristics of pure Mg and Mg−14Li alloy, electrochemical equivalent circuit models (inserted in Figs. 4(a) and (b)) are proposed to fit the EIS data and the fitted results are listed in Table 1. In the equivalent circuits, R_s is solution resistance; R_t and Q_{dl} represent charge transfer resistance and electric double layer, respectively, at the interface between substrate and electrolyte; Q_{dl} is defined by Y_{dl} and n_{dl}, if n_{dl}=1, Q_{dl} is identical to a capacitor, and if n_{dl}=0, Q_{dl} represents a resistance; R_f and Q_f (defined by Y_f and n_f) represent film resistance and capacity in the low frequency capacitance loop, respectively. The R_t values of the two specimens increase with immersion time, but the R_t values of pure Mg are consistently larger than those of Mg−14Li alloy for a certain immersion time, implying the better corrosion resistance of pure Mg.

3.3 Surface film

SONG et al [31] found that for the HCP Mg−Zn alloy, a compact corrosion product film formed during the initial stage of immersion (less than 2 h), and then the film gradually degraded due to dissolution reaction. Moreover, Mg−5Zn alloy containing more second phases accelerated the occurrence of a broken surface film compared with Mg−2Zn alloy with less second phases [31]. For BCC Mg−10.95Li−3.29Al−0.59Y−0.19Zr alloy containing second phases, the surface film can maintain its protective function even it was scratched or at a positive loading over-potential of

Table 1 Fitted EIS data on basis of equivalent circuits presented in Fig. 4

Sample	Conditioning time	R_s/ ($\Omega\cdot cm^2$)	Y_{dl}/ ($\mu\Omega^{-1}\cdot cm^{-2}\cdot s^n$)	n_{dl}	R_t/ ($\Omega\cdot cm^2$)	Y_f/ ($\mu\Omega^{-1}\cdot cm^{-2}\cdot s^n$)	n_f	R_f/ ($\Omega\cdot cm^2$)
Pure Mg	10 min	70±0.6	13.0±2.4	0.94±0.02	1375±13	867±29	0.51±0.04	1206±46
	8 h	72±0.8	12.5±1.5	0.92±0.01	1828±36	809±18	0.64±0.02	1334±21
	16 h	68±0.5	12.5±1.8	0.92±0.01	2605±46	797±22	0.70±0.02	1468±18
Mg−14Li	10 min	89±0.8	33.2±3.4	0.92±0.02	778±48	3053±253	0.72±0.03	324±33
	8 h	90±1.2	33.7±3.4	0.86±0.03	1593±117	2461±195	0.88±0.04	492±53
	16 h	80±0.7	45.1±3.5	0.85±0.07	1803±213	2155±26	0.89±0.02	511±19

50 mV [22]. Therefore, it can be speculated that the cathodic second phases are generally detrimental to the $Mg(OH)_2$ film of traditional HCP Mg. However, it is hard to destroy the resilient Li_2CO_3 film on BCC Mg−Li during immersion in NaCl. In this work, a pure matrix without second phases contributes to the prolonging life span of an intact $Mg(OH)_2$ film on pure Mg. To further compare the morphologies and composition of the surface film on the HCP and BCC magnesium specimens, the SEM images and Raman testing results of the surface film (planar and cross-sectional) on the pure Mg and the Mg−14Li alloy after 8 h immersion are shown in Fig. 5. Typical flake-like $Mg(OH)_2$ particles are observed on the pure Mg, as reported in previous work [31]. However, the cross-sectional film is barely observed on the pure Mg, which is ascribed to limited $Mg(OH)_2$ (combined with MgO) compounds deposited on the HCP Mg. The outer $Mg(OH)_2$ layer is typical with thickness of 500 nm, and the inner MgO layer is only 50−90 nm [34−36]. After 8 h immersion, the corrosion film on the pure Mg is very thin and cannot be properly observed on cross-sections by SEM. Nevertheless, previous works have systematically characterized the surface film on magnesium and confirmed the existence of $Mg(OH)_2$ and MgO layers via transmission electron microscopy (TEM) at nano-scale [35].

The primary composition of the surface film on pure Mg can be determined as $Mg(OH)_2$ detected

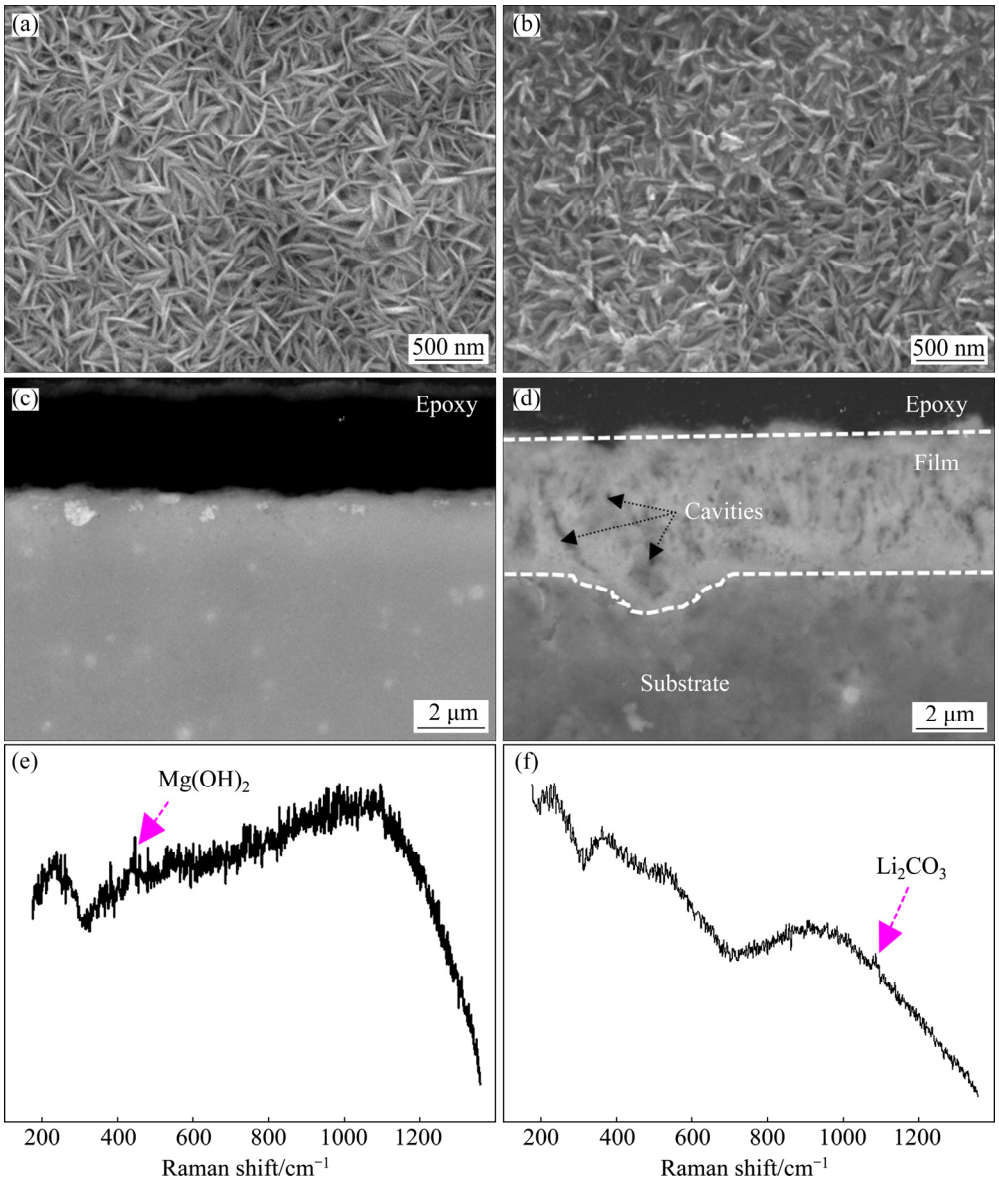

Fig. 5 Planar (a, b) and cross-sectional (c, d) morphologies and Raman analysis (e, f) of surface film on pure Mg (a, c, e) and Mg−14Li alloy (b, d, f) exposed to 0.1 mol/L NaCl for 8 h

via Raman spectroscopy even though its peak is weak (Fig. 5(e)). For Mg−14Li alloy, the morphology of the surface film presents articulated need-like particles that are evidently different from the flake-like $Mg(OH)_2$ particles. Meanwhile, the thickness of the surface film on Mg−14Li is up to 4 μm, but some fine cavities are doped, indicating the possible occurrence of permeated corrosive media in the film. As a result, the thick film can still be broken down with prolonging immersion time (Fig. 2(d)). On the other hand, the addition of lithium (with high chemical activity) can facilitate the formation of the surface film due to the rapid ion exchange (deposition) occurring on the surface. Furthermore, lithium existing in the sub-surface can transfer into the outmost surface, resulting in an enriched Mg inner-layer under the outmost layer [23,24]. The primary composition of the surface film on Mg−14Li is defined as Li_2CO_3 compounds based on Raman spectroscopy (Fig. 5(f)). Therefore, the addition of lithium with high chemical activity can alter the surface film on Mg, including the morphology and composition, whilst the thick protective film is not optimal for the binary BCC Mg−Li as it consumes much more substrate. The possible regulating and controlling surface film on Mg−Li alloys will be researched in our future study.

The surface film forming dynamically on the pure Mg and Mg−14Li alloy during potentiodynamic polarization is characterized by Raman spectroscopy in real time (the schematic of the special cell system is shown in Fig. 6(a)) and the testing points are denoted on the schematic φ–J plot (Fig. 6(b)). The corresponding Raman results are shown in Figs. 6(c) and (d). As the fluorescence is caused by the thin electrolyte (containing water) on the surface of the sample [37], two peaks at about 320 and 490 cm^{-1} always emerge, annihilating the information of limited $Mg(OH)_2$ (located at about 300 and 450 cm^{-1}) [38]. Moreover, the Raman spectra corresponding to the location of carbonate are consistently flat for pure HCP Mg, indicating that only a limited amount of carbonate compounds can be deposited on the surface of pure Mg during polarization. Furthermore, a thin layer of $Mg(OH)_2$

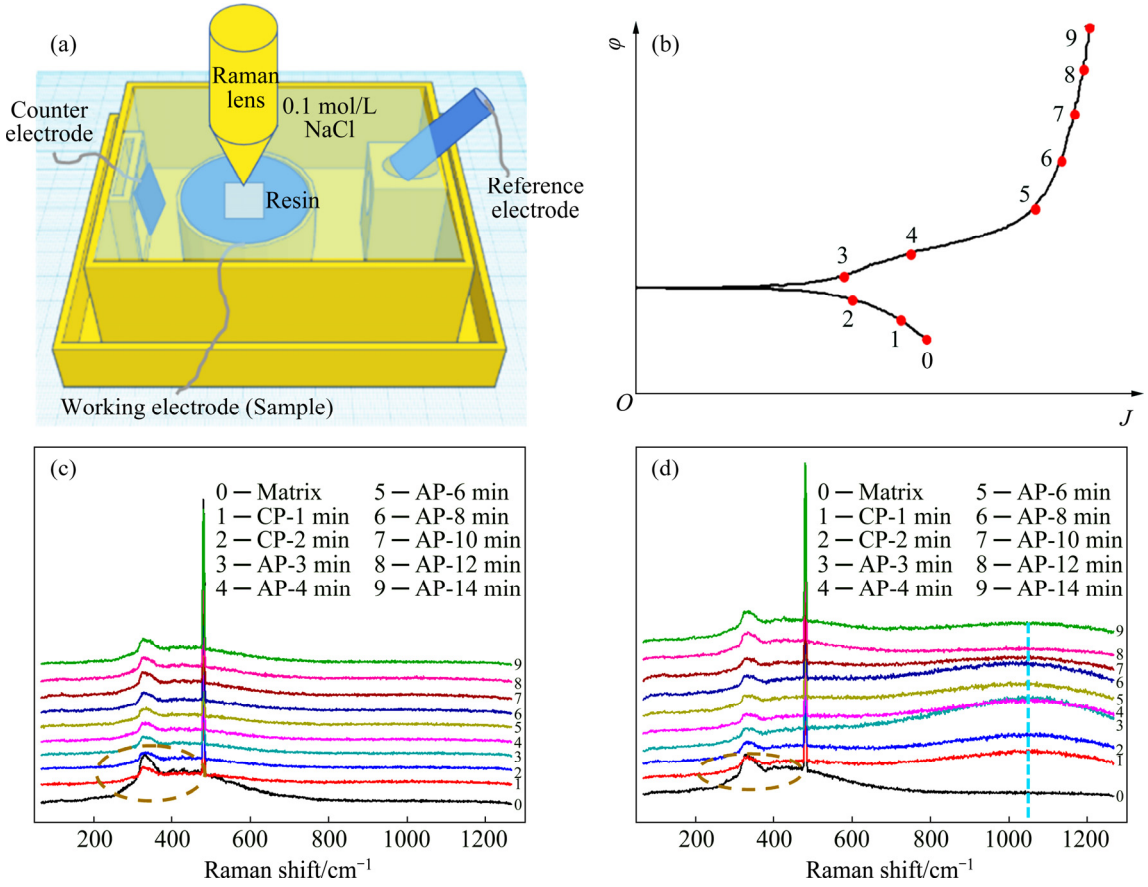

Fig. 6 Schematic in-situ configuration of electrochemical-Raman tests (a), testing points on schematic φ–J plot (b), and corresponding results of pure Mg (c) and Mg−14Li alloy (d) during potentiodynamic polarization in 0.1 mol/L NaCl

is not detected on the pure Mg or it is overlapped by the fluorescence effect. However, it is still rational to evaluate the Li_2CO_3 compounds on Mg−14Li alloy located at about 1100 cm^{-1} [38]. It can be seen that Li_2CO_3 compounds are not deposited on the Mg−14Li alloy during cathodic polarization as no vibration is detected on the Raman spectra (Curves 0−2), while the Li_2CO_3 vibration is apparent when a low anodic potential is applied (Curves 3 and 4). When the anodic potential is further elevated, the Li_2CO_3 vibration disappears (Curves 5−9), implying that the Li_2CO_3 surface film can only form at a proper potential. In essence, the cathodic over-potential inhibits the formation of Li_2CO_3 and the high anodic over-potential can accelerate its dissolution [21]. Therefore, a Li_2CO_3 film can form dynamically on the BCC Mg−Li, especially at a low anodic potential, resulting in an essential difference in the surface film with that on the traditional Mg.

It is apparent that a pure or single Li_2CO_3 film on the pure BCC Mg−Li matrix does not contribute to the high corrosion resistance of alloying BCC Mg−Li as its protective function is inferior to that of a pure or single $Mg(OH)_2$ film on pure Mg. The protective film on BCC Mg−Li alloys is composed of complicated compounds instead of the single Li_2CO_3, and the film can be optimized through alloying and/or processing. The effect of the crystal structure of pure HCP Mg and BCC Mg−14Li alloy on the corrosion behavior and surface film is considered theoretically in this work. However, the change in the corrosion performance and surface film due to the crystal structure in the magnesium system is not as large as the effect of altering the bulk alloy chemistry, as reported in the previous work [39]. Thus, the chemical or electrochemical properties of the alloying elements in the matrix determine the corrosion resistance and surface film of magnesium.

4 Conclusions

(1) The corrosion resistance of pure Mg covered with flake-like $Mg(OH)_2$ film is superior to that of Mg−14Li alloy covered with articulated needle-like Li_2CO_3 film.

(2) The Li_2CO_3 film deposited on the surface is defined using a static and dynamic Raman technique combined with immersion and electrochemical testing. The Li_2CO_3 film with some cavities allows the permeation of corrosive ions and dissolves under a high applied anodic potential.

(3) The protective function of unalloyed Li_2CO_3 film, which consumes much more substrate, is not the most ideal for magnesium, but guides a possible way for regulating the film containing Li_2CO_3 and/or other compounds through alloying.

References

[1] SUN Yue-hua, WANG Ri-chu, PENG Chao-qun, FENG Yan, YANG Ming. Recent progress in Mg−Li matrix composites [J]. Transactions of Nonferrous Metals Society of China, 2019, 29: 1−14.

[2] OUYANG Si-jie, LIU Wen-cai, WU Guo-hua, JI Hao, GAO Zhan-kui, PENG Xiang, LI Zhong-quan, DING Wen-jiang. Microstructure and mechanical properties of as-cast Mg−8Li−*x*Zn−yGd (*x*=1, 2, 3, 4; *y*=1, 2) alloys [J]. Transactions of Nonferrous Metals Society of China, 2019, 29: 1211−1222.

[3] SUN Yue-hua, WANG Ri-chu, PENG Chao-qun, FENG Yan, YANG Ming. Corrosion behavior and surface treatment of superlight Mg−Li alloys [J]. Transactions of Nonferrous Metals Society of China, 2017, 27: 1455−1475.

[4] WANG Bao-jie, LUAN Ji-yu, XU Dao-kui, SUN Jie, LI Chuan-qiang, HAN En-hou. Research progress on the corrosion behavior of magnesium-lithium-based alloys: A review [J]. Acta Metallurgica Sinica (English Letters), 2019, 32: 1−9.

[5] WANG Zhi-hu, ZHANG Ju-mei, LI Yan, BAI Li-jing, ZHANG Guo-jun. Enhanced corrosion resistance of micro-arc oxidation coated magnesium alloy by superhydrophobic Mg−Al layered double hydroxide coating [J]. Transactions of Nonferrous Metals Society of China, 2019, 29: 2066−2077.

[6] TAHERI M, PHILLIPS R C, KISH J R, BOTTON G A. Analysis of the surface film formed on Mg by exposure to water using a FIB cross-section and STEM−EDS [J]. Corrosion Science, 2012, 59: 222−228.

[7] SANTAMARIA M, QUARTO F D, ZANNA S, MARCUS P. Initial surface film on magnesium metal: A characterization by X-ray photoelectron spectroscopy (XPS) and photocurrent spectroscopy (PCS) [J]. Electrochimica Acta, 2017, 53: 1314−1324.

[8] ZENG Rong-chang, SUN Lu, ZHENG Yu-feng, CUI Hong-zhi, HAN En-hou. Corrosion and characterisation of dual phase Mg−Li−Ca alloy in Hank's solution: The influence of microstructural features [J]. Corrosion Science, 2014, 79: 69−82.

[9] XU Chun-hua, GAO Wei. Pilling−Bedworth ratio for oxidation of alloys [J]. Material Research Innovations, 2000, 3(4): 231−235.

[10] WANG Bao-jie, XU Dao-kui, WANG Shi-dong, SHENG Li-yuan, ZENG Rong-chang, HAN En-hou. Influence of solution treatment on the corrosion fatigue behavior of an as-forged Mg−Zn−Y−Zr alloy [J]. International Journal of

Fatigue, 2019, 120: 46−55.

[11] WANG Bao-jie, XU Dao-kui, SUN Jie, HAN En-hou. Effect of grain structure on the stress corrosion cracking (SCC) behavior of an as-extruded Mg−Zn−Zr alloy [J]. Corrosion Science, 2019, 157: 347−356.

[12] NOURI M, LIU Zi-ran, LI Dong-yang, YAN Xiao-guo, TAHREEN N, CHEN Dao-lun. The role of minor yttrium in tailoring the failure resistance of surface oxide film formed on Mg alloys [J]. Thin Solid Films, 2016, 615: 29−37.

[13] WANG Bao-jie, XU Dao-kui, WANG Shi-dong, HAN En-hou. Recent progress in the research about fatigue crack initiation of Mg alloys under elastic stress amplitudes: A review [J]. Frontiers of Mechanical Engineering, 2019, 14: 113−127.

[14] WANG Bao-jie, XU Dao-kui, SHENG Li-yuan, HAN En-hou, SUN Jie. Understanding to the deformation and fracture mechanisms of an annealing-tailored “bimodal” grain-structured Mg alloy [J]. Journal of Materials Science & Technology, 2019, 35: 2423−2429.

[15] YANG Jun-jie, BLAWERT C, LAMAKA S V, YASAKAU K A, WANG Li, LAIPPLE D, SCHIEDA M, DI Shi-chun, ZHELUDKEVICH M L. Corrosion inhibition of pure Mg containing a high level of iron impurity in pH neutral NaCl solution [J]. Corrosion Science, 2018, 142: 222−237.

[16] CAI Chang-hong, SONG Ren-bo, WANG Luan-xiang, LI Jing-yuan. Effect of anodic *T* phase on surface micro-galvanic corrosion of biodegradable Mg−Zn−Zr−Nd alloys [J]. Applied Surface Science, 2018, 462: 243−254.

[17] GAO Jia-sheng, WU Sha, QIAO Li-ying, WANG Yong. Corrosion behavior of Mg and Mg−Zn alloys in simulated body fluid [J]. Transactions of Nonferrous Metals Society of China, 2008, 18: 588−592.

[18] XU Tian-cai, YANG Yan, PENG Xiao-dong, SONG Jiang-feng, PAN Fu-sheng. Overview of advancement and development trend on magnesium alloy [J]. Journal of Magnesium and Alloys, 2019, 7(3): 536−544.

[19] MAJD A M, FARZINFAR M, PASHAKHANLOU M, NAYYERI M J. Effect of RE elements on the microstructural and mechanical properties of as-cast and age hardening processed Mg−4Al−2Sn alloy [J]. Journal of Magnesium and Alloys, 2018, 6(3): 309−317.

[20] XU Wan-qiang, BIRBILIS N, SHA Gang, WANG Yu, DANIELS J, XIAO Yang, FERRY M. A high-specific-strength and corrosion-resistant magnesium alloy [J]. Nature Materials, 2015, 14: 1229−1235.

[21] LI Chuan-qiang, XU Dao-kui, CHEN Xiao-bo, WANG Bao-jie, WU Rui-zhi, HAN En-hou, BIRBILIS N. Composition and microstructure dependent corrosion behaviour of Mg−Li alloys [J]. Electrochimica Acta, 2018, 260: 55−64.

[22] YAN Yuan-ming, ZHOU Peng, GHARBI O, ZENG Zhuo-ran, CHEN Xiao-bo, VOLOVITCH P, OGLE K, BIRBILIS N. Investigating ion release using inline ICP during in situ scratch testing of an Mg−Li(−Al−Y−Zr) alloy [J]. Electrochemistry Communication, 2019, 99: 46−50.

[23] YAN Yuan-ming, GHARBI O, MALTSEVA A, CHEN Xiao-bo, ZENG Zhuo-ran, XU Shi-wei, XU Wan-qiang, VOLOVITCH P, FERRY M, BIRBILIS N. Investigating the structure of the surface film on a corrosion resistant Mg−Li(−Al−Y−Zr) alloy [J]. Corrosion, 2019, 75(1): 89−89.

[24] YAN Yuan-ming, QIU Yao, GHARBI O, BIRBILIS N. NAKASHIMA P N H. Characterisation of Li in the surface film of a corrosion resistant Mg−Li(−Al−Y−Zr) alloy [J]. Applied Surface Science, 2019, 494: 1066−1071.

[25] LIU Wei, YIN Zhou-lan, DING Zhi-ying. Low-temperature phase transitions of sodium aluminate solutions [J]. Transactions of Nonferrous Metals Society of China, 2019, 29: 194−199.

[26] ESMAILY M, SVENSSON J E, FAJARDO S, BIRBILIS N, FRANKEL G S, VIRTANMEN S, ARRABAL R, THOMAS S, JOHANSSON L G. Fundamentals and advances in magnesium alloy corrosion [J]. Progress in Materials Science, 2017, 89: 92−193.

[27] SUDHOLZ A D, KIRKLAND N T, BUCHHEIT R G, BIRBILIS N. Electrochemical properties of intermetallic phases and common impurity elements in magnesium alloys [J]. Electrochemical and Solid-state Letters, 2011, 14(2): C5−C7.

[28] THOMAS S, GHARBI O, SALLEH S H, VOLOVITCH P, OGLE K, BIRBILIS N. On the effect of Fe concentration on Mg dissolution and activation studied using atomic emission spectroelectrochemistry and scanning electrochemical microscopy [J]. Electrochimica Acta, 2016, 210: 271−284.

[29] ZHAO Chen, CAO Fu-yong, SONG Guang-ling. Corrosivity of haze constituents to pure Mg [J]. Journal of Magnesium and Alloys, 2020, 8(1): 150−162.

[30] ZHANG Xu-ming, WU Guo-song, PENG Xiang, LI Li-min, FENG Hong-qing, GAO Biao, HUO Kai-fu, CHU P K. Mitigation of corrosion on magnesium alloy by predesigned surface corrosion [J]. Scientific Reports, 2015, 5: 17399.

[31] SONG Ying-wei, HAN En-hou, DONG Kai-hui, SHAN Da-yong, YIM C D, YOU B S. Study of the corrosion product films formed on the surface of Mg−*x*Zn alloys in NaCl solution [J]. Corrosion Science, 2014, 88: 215−225.

[32] LI Chuan-qiang, XU Dao-kui, ZENG Zhuo-ran, WANG Bao-jie, SHENG Li-yuan, CHEN Xiao-bo, HAN En-hou. Effect of volume fraction of LPSO phases on corrosion and mechanical properties of Mg−Zn−Y alloys [J]. Materials & Design, 2017, 121: 430−441.

[33] CHENG Yuan-fen, DU Wen-bo, LIU Ke, FU Jun-jian, WANG Zhao-hui, LI Shu-bo, FU Jin-long. Mechanical properties and corrosion behaviors of Mg−4Zn−0.2Mn−0.2Ca alloy after long term in vitro degradation [J]. Transactions of Nonferrous Metals Society of China, 2020, 30(2): 363−372.

[34] LI Chuan-qiang, XU Dao-kui, ZHANG Zheng-rong, HAN En-hou. Influence of the lithium content on the negative difference effect of Mg−Li alloys [J]. Journal of Materials Science & Technology, 2020, 57: 138−145.

[35] TAHERI M, PHILLIPS R C, KISH J R, BOTTON G A. Analysis of the surface film formed on Mg by exposure to water using a FIB cross-section and STEM−EDS [J]. Corrosion Science, 2012, 59: 222−228.

[36] BLAND L G, GUSIEVA K, SCULLY J R. Effect of crystallographic orientation on the corrosion of magnesium: comparison of film forming and bare crystal facets using electrochemical impedance and Raman spectroscopy [J]. Electrochimica Acta, 2017, 227: 136−151.

[37] CAREY D M, KORENOWSKI G M. Measurement of the Raman spectrum of liquid water [J]. The Journal of Chemical Physics, 1998, 108: 2669−2675.
[38] Database of Raman Spectra, X-ray Diffraction and Chemistry Data [EB/OL]. http://rruff.info/.
[39] XIA Xiao-jian, DAVIES C H J, NIE Jian-feng, BIRBILIS N. The influence of composition and processing on the corrosion of magnesium alloys containing binary and ternary additions of zinc and strontium [J]. Corrosion, 2015, 71(1): 38−49.

纯镁和 Mg−14Li 合金耐蚀性与表面膜的对比

李传强，童之沛，何溢斌，黄怀沛，董 勇，张 鹏

广东工业大学 材料与能源学院，广州 510006

摘 要：采用析氢实验、失重实验、电化学实验、原位电化学拉曼光谱实验以及显微组织观察(光学与扫描电子显微镜)等实验方法，对比研究密排六方结构(HCP)的纯镁和体心立方结构(BCC)的二元 Mg−14Li 合金(质量分数，%)在 0.1 mol/L NaCl 溶液中的腐蚀行为与表面膜结构。实验结果表明：纯镁的耐蚀性优于 Mg−14Li 合金的，并且两种材料表面膜的保护功能均随着浸泡时间(16 h 内)的延长而提高。通过扫描电子显微形貌分析，发现不同于纯镁表面形成的较薄且呈片状的 $Mg(OH)_2$ 膜层，Mg−14Li 合金表面形成较厚且呈交织针状含有 Li_2CO_3 的膜层；然而，两种材料的表面膜均在高的阳极过电位下发生破损。因此，两种材料的不同腐蚀抗性可归功于在其表面形成不同的保护膜。

关键词：镁锂合金；腐蚀抗性；表面膜；电化学测试；原位电化学拉曼光谱

(Edited by Bing YANG)